# Ammonia emission estimates using CrIS satellite observations over Europe

Jieying Ding[1*], Ronald van der A[1], Henk Eskes[1], Enrico Dammers[2], Mark Shephard[3], Roy Wichink Kruit[4], Marc Guevara[5], Leonor Tarrason[6]

1. Royal Netherlands Meteorological Institute (KNMI), De Bilt, The Netherlands

2. Netherlands Organisation for Applied Scientific Research (TNO), Utrecht, The Netherlands

3. Environment and Climate Change Canada (ECCC), Toronto, Ontario, Canada

4. National Institute for Public Health and the Environment, Bilthoven, The Netherlands

5. Barcelona Supercomputing Center, Barcelona, Spain

6. NILU – Norwegian Institute for Air Research, Kjeller, Norway

*Corresponding authors: Jieying Ding (jieying.ding@knmi.nl)

## Abstract

Over the past century ammonia ($NH_3$) emissions have increased with the growth of livestock and fertilizer usage. The abundant $NH_3$ emissions lead to secondary fine particulate matter ($PM_{2.5}$~~PM2.5~~) pollution, climate change, reduction in biodiversity and affect~~s~~ human health. Up-to-date and spatially and temporally resolved information of $NH_3$ emissions is essential to better quantify its impact. In this study we applied the existing DECSO (Daily Emissions Constrained by Satellite Observations) algorithm to $NH_3$ observations from the Cross-track Infrared Sounder (CrIS) to estimate $NH_3$ emissions. Because $NH_3$ in the atmosphere is influenced by Nitrogen Oxides ($NO_x$), we implemented DECSO to estimate $NO_x$ and $NH_3$ emissions simultaneously. The emissions are derived over Europe for 2020 on a spatial resolution of 0.2° × 0.2° using daily observations from both CrIS and TROPOMI (on the Sentinel 5p satellite). Due to the ~~sparseness~~ limited number of daily satellite observations of $NH_3$, monthly emissions of $NH_3$ are reported. The total $NH_3$ emissions derived from observations are about 8 Tg/year with a precision of about 5-17~~0.2~~ % per grid cell per year over the European domain [-10° ~30° E, 35° ~ 55° N]. The comparison of the satellite-derived $NH_3$ emissions from DECSO with independent

bottom-up inventories and in-situ observations indicates a consistency in terms of magnitude on the country totals, the results also being comparable regarding the temporal and spatial distributions. The validation of DECSO over Europe implies that we can use DECSO to quickly derive fairly good monthly emissions of $NH_3$ over regions with limited local information of $NH_3$ emissions.

## 1 Introduction

Ammonia ($NH_3$) is the most abundant alkaline gas and one of the main reactive nitrogen species in the atmosphere. $NH_3$ is a precursor for the formation of atmospheric aerosols, which play an important role in climate change. In Europe, about 50% (Wyer et al., 2022) of atmospheric $NH_3$ is transformed into fine particulate matter ($PM_{2.5}$~~PM2.5~~) composed of ammonium through chemical reactions with sulfuric and nitric acids from nitrogen oxides ($NO_x$) and sulphur dioxides ($SO_2$) in the atmosphere (Renard et al., 2004; Schaap et al., 2004). According to the European Environment Agency (EEA), the dominant source of $NH_3$ in Europe is agriculture, which was responsible for more than 90% of the European emissions. The other source sectors include industry, transport, energy, waste treatment and biomass burning (Behera et al., 2013; Backes et al., 2016a; Van Damme et al., 2018; Adams et al., 2019). Excessive $NH_3$ emissions have adverse impact on biodiversity, human health, and climate change (Galloway et al., 2008). Over the past century, $NH_3$ emissions increased strongly with the growing human population, cattle farming and fertilizer usage (Crippa et al., 2023; Erisman et al., 2008; Van Damme et al., 2021), leading to high nitrogen deposition loads to water and soil (Erisman et al., 2013) with the associated eutrophication, acidification and biodiversity loss problems (Behera et al., 2013). Since 2019, the Dutch policy makers paid a lot of attention to $NH_3$ emissions due to the nitrogen (N) crisis after the national programmatic approach to nitrogen was rejected by the supreme court, because it was inadequate for the protection of vulnerable nature areas (named Natura 2000). The Dutch government is obliged by EU laws to protect the natural environment and prevent damage caused by too high emissions of reactive nitrogen. Studies show~~s~~ that abatement of $NH_3$ emissions is very cost-effective to improve air quality and have high social benefits (Backes et al., 2016b; Zhang et al., 2020; Gu et al., 2021). Detailed spatially and temporally resolved information of $NH_3$ emissions is crucial for both scientific communities and policy makers to study and predict pollutant concentrations and deposition with their impact on the environment and to motivate environmental control strategies.

The empirical method to estimate $NH_3$ emissions is the so-called bottom-up approach, which combines available official reported activity data incorporating a full differentiation of emission activities with emission factors, and technology and abatement measures from individual countries for each source category (Crippa et al., 2018; Crippa et al., 2023; Janssens-Maenhout et al., 2019). The annual emissions are then distributed in time and space based on proxy data such as land use data, and meteorological parameters (Backes et al., 2016a). Ge et al. (2020) summarized the key factors of agricultural $NH_3$ emissions: local agricultural practices, ~~method of~~ manure and fertilizer application including type, amount and method, animal ~~type~~species, housing ~~type~~, manure storage ~~type~~, meteorological conditions, soil ~~conditions~~properties, and regulations of agricultural practice. The uncertainties of $NH_3$ emissions calculated by the bottom-up approach are very large due to insufficient data on agricultural activities (Behera et al., 2013; Beusen et al., 2008). Crippa et al. (2018) pointed out that the uncertainty of $NH_3$ (between 186 % and 294.4 %) in the EDGAR (The Emissions Database for Global Atmospheric Research) inventory is the largest among all pollutants because of the high uncertainty of both agricultural statistics and emission factors.

The validation of $NH_3$ emission inventories using ground-based observations is very challenging due to the sparsely distributed in-site measurement network. $NH_3$ concentrations have large temporal and spatial variability due to its short lifetime, which ranges from about a few hours to two days (Dammers et al., 2019; Luo et al., 2022). Densely distributed hourly or daily ground measurements are impractical for large areas due to high costs and specific operational requirements (Noordijk et al., 2020). In the last decade, a wide spatial and temporal coverage of satellite observations of $NH_3$ in lower troposphere was established due to the development of infrared nadir viewing satellite instruments, such as the Tropospheric Emission Spectrometer (TES) (Beer et al., 2008) on the NASA Aura satellite. The operational Cross-track Infrared Sounder (CrIS) (Shephard and Cady-Pereira, 2015) on the Suomi National Polar-orbiting Partnership (S-NPP) and on the Joint Polar Satellite System-1 and System-2 (JPSS-1 and JPSS-2, also named as NOAA-20 and NOAA-21) satellites of NASA/NOAA, and the Infrared Atmospheric Sounder Interferometer (IASI) (Clarisse et al., 2009) on the MetOp satellites from the European Space Agency (ESA), with their large swaths, provide daily global coverage of $NH_3$ observations and improve our understanding of $NH_3$ global distribution and temporal variability.

$NH_3$ emissions can be obtained by applying an inversion algorithm to satellite observations. Such estimates provide useful information which is independent from bottom-up inventories. By using IASI $NH_3$ observations, Van Damme et al. (2018) identified $NH_3$ emission hotspots and calculated emissions based on a mass balance approach. They found that $NH_3$ emissions of most hotspots, especially industrial emitters, were largely underestimated compared to EDGAR. Dammers et al. (2019) used both IASI and CrIS observations to derive emissions, lifetimes and plume widths of $NH_3$ from large agricultural and industrial point sources and concluded that 55 locations were missing in the Hemispheric Transport Atmospheric Pollution version 2 (HTAPv2) emission inventory. Besides the studies on point sources, data assimilation techniques combining a chemical transport model (CTM) with satellite observations are also widely used to derive $NH_3$ surface emissions. van der Graaf et al. (2022) adjusted the $NH_3$ emissions over Europe using a local ensemble transport Kalman filter (LETKF) applied to CrIS $NH_3$ profiles. Sitwell et al. (2022) developed an ensemble-variational inversion system to estimate $NH_3$ emissions from CrIS over North America. Another widely used method is 4D-Var using the GEOS-Chem global chemistry transport model, which has been applied to America, China and Europe using $NH_3$ observation from different instruments (Zhu et al., 2013; Zhang et al., 2018; Li et al., 2019; Cao et al., 2020; Chen et al., 2021; Cao et al., 2022). The main advantage of CrIS is the combination of global coverage and the improved sensitivity in the boundary layer attributed to the low spectral noise of about 0.04 K at 280 K in the $NH_3$ spectral band (Zavyalov et al., 2013). The infrared instrument is also more sensitive at the overpass time in the early afternoon with high thermal contrast between air and surface.

The Daily Emissions Constrained by Satellite Observations (DECSO) inversion algorithm uses satellite column observations to derive emissions for short-lived gases based on an extended Kalman Filter (Mijling and van der A, 2012). The concentrations of the species are calculated from the emissions by a CTM and compared to satellite observations. One of the main advantages to use DECSO is the fast calculation speed compared to other data assimilation methods. Furthermore, the derived emissions are updated by addition, not by scaling the existing emissions. This enables the fast detection of new sources and changed emissions. In previous studies, DECSO has been applied to nitrogen dioxide ($NO_2$) observations from different satellites and uses the Eulerian regional off-line CTM CHIMERE (Menut et al., 2021; Menut et al., 2013) to estimate regional NOx ($NO_2$+NO) emissions and it revealed that the temporal and spatial variability of total surface $NO_x$ emissions are well captured by DECSO compared to bottom-up inventories or in-situ observations (Ding et al., 2015; Ding et al., 2017b; Ding et al., 2020; van der A et al., 2020; Ding et al., 2022; Liu et al., 2018).

Direct validation of emission inventories, regardless of bottom-up or satellite-derived approaches, presents the same challenge due to the inherent difficulty of directly measuring large-scale emissions on the ground. The intercomparison of emissions using independent data and different approaches are usually performed to assess the emission data. Another common way to validate~~ion~~ emissions can be achieved by using them as input data in a chemical transport model. The model simulated concentrations are compared to in-situ observations.

In this study we extend the DECSO-NOx system to $NH_3$ in order to derive both $NO_x$ and $NH_3$ emissions simultaneously, using CrIS $NH_3$ observations and $NO_2$ observations from the TROPOspheric Monitoring Instrument (TROPOMI) (Veefkind et al., 2012). Using the multi-species DECSO version, we update $NO_x$ and $NH_3$ emissions simultaneously to reduce the impact of the temporal change (e.g. trend) of $NO_x$ when deriving $NH_3$ emissions. After the description of the DECSO algorithm applied to $NH_3$, the results of $NH_3$ emissions over Europe are presented at a spatial resolution of 0.2° × 0.2°. To evaluate the derived $NH_3$ emissions, we will compare the country totals and the monthly variability with bottom-up inventories with a focus on $NH_3$ emissions in the Netherlands. In addition, we compare the $NH_3$ concentration simulations of CHIMERE using different emission inventories with in-situ observations.

# 2 Data and Method

## 2.1 Satellite observations

### *2.1.1 CrIS observations of $NH_3$*

The CrIS instrument is a Fourier transform spectrometer (FTS) launched on the Suomi National Polar-orbiting Partnership (SNPP) satellite in 2011 and on the NOAA-20 satellite in 2017. The overpass time of SNPP at the equator is about 01:30 and 13:30 local time. NOAA-20 circles the earth in the same orbit as SNPP, but it is separated in time and space by 50 minutes and crosses the equator at about 02:20 and 14:20 local time. The instrument has a wide swath of up to 2200 km providing twice daily global coverage. The total angular field-of-view consists of a 3×3 array of circular pixels of 14 km diameter each at nadir (Han et al., 2013). CrIS measures the infrared spectrum including the main $NH_3$ spectral signatures located in the longwave window region between 900 and 1000 $cm^{-1}$. The spectral resolution of the radiance data is 0.625 $cm^{-1}$. $NH_3$ observations are retrieved with the CrIS Fast Physical Retrieval (CFPR) algorithm based on an optimal estimate method minimizing the difference between measured spectral radiances and those simulated by a radiative transfer model (Shephard and Cady-Pereira, 2015). Three typical a priori profiles of $NH_3$ representing high-source, moderate-source and background source are used in the retrieval algorithm. The $NH_3$ profiles are retrieved on 14 pressure levels with the peak sensitivity of CrIS between 900 and 700 hPa (Shephard et al., 2020). For SNPP, the retrieval products start from 2011 and ends in May 2021 with missing data from April to August in 2019. The $NH_3$ retrieval product of NOAA-20 starts from March 2019. We use the version 1.6.4 retrieval products of CrIS on both SNPP and NOAA-20 from September 2019 to December 2020, which also accounts for non-detects in the observations and retrievals through optically thin clouds (White et al., 2023). We use the daytime observations with the quality flag larger than 3 over our study domain of Europe [-10° ~30° E, 35° ~ 55° N] (Shephard et al., 2020). Since there are almost no emissions over ocean, we only use the observations over land. To reduce extreme emission updates in one day we filter the $NH_3$ data larger than the value at $99^{th}$ percentile of all observations for the selected period over the study domain. This has also been applied by van der Graaf et al. (2022). To make a fair comparison between $NH_3$ observations of CrIS and model simulations of CHIMERE, we interpolate modelled concentrations from the model grid cell over the satellite footprints and apply the averaging kernel to the modelled profile. Although the $NH_3$ observations from CrIS are in circular pixels, we still assume the pixel to be rectangular and calculate the pixel corner coordinates based on the satellite height, satellite zenith angle and viewing angle assuming the width of the pixel to be equal to the diameter of the circular pixel. To simplify the calculation of applying the original logarithmic averaging kernels, we converted them to linearized average kernels based on the method of Cao et al. (2022).

### 2.1.2 TROPOMI observations of $NO_2$

TROPOMI is onboard the Sentinel-5 Precursor (S5P) satellite launched on 13 October 2017 with the high spatial resolution of 3.5 × 5.5 $km^2$ at nadir for the $NO_2$ observations. The overpass time is about 13:30 local time, similar as for CrIS. We use TROPOMI tropospheric $NO_2$ columns from the version 2.4 reprocessed retrieval dataset (van Geffen et al., 2022) and follow the recommendations for using the QA value as detailed in the Product User Manual (Eskes and Eichmann, 2022). $NO_2$ columns are converted into 'super-observations' representing the integrated average (Boersma et al., 2016; Rijsdijk et al., 2024) over the 0.2° × 0.2° grid cells. The super-observation error takes into account spatial correlations between individual TROPOMI observations and representativity errors in the case of incomplete coverage. In this paper, the super-observations are calculated for the $NO_2$ columns from surface till about 700hPa where the $NO_2$ concentrations are most related to surface emissions. The signal-to-noise ratio and calculation time of DECSO are improved by using super-observations. The details of TROPOMI $NO_2$ data used by DECSO are described in Ding et al. (2020) and van der A et al. (2024).

## 2.2 Ground-based observations.

To evaluate the $NH_3$ emissions derived by DECSO, we use independent ground-based observations in 2020 to compare with model simulated $NH_3$ concentrations of CHIMERE using different inventories. Compared to other countries, Netherlands has the densest network for monitoring surface $NH_3$ concentrations. We use hourly $NH_3$ concentrations measured by mini-DOAS at six locations (Figure S1) from the Dutch Monitoring Air Quality (LML) network (Berkhout et al., 2017) and monthly measurements of $NH_3$ concentration provided by passive samples at 394 locations (Figure S2) from the Dutch Measuring Ammonia in Nature (MAN) network (Lolkema et al., 2015). The uncertainty in $NH_3$ concentrations measured with individual passive samples is large (22% for a single monthly measurement) and the measurements are calibrated monthly against the high-quality measurements (about 20% for an hourly measurement) from the LML network to enhance the accuracy.

## 2.3 Emission inventories

To verify the satellite-derived emissions of $NH_3$ in Europe, we compare them to several emission inventories including: the national emissions inventories officially reported under the Convention on

Long-range Transboundary Air Pollution (LRTAP) (Pinteris, 2023) of 2020, the emissions reported under the European Pollutant Release and Transfer Register (E-PRTR) (EPRTR, 2012) of 2020 including releases from industrial facilities and livestock facilities, the global emission inventory Hemispheric Transport of Air Pollution (HTAP) v3 of 2018 (Crippa et al., 2023), the Copernicus Atmosphere Monitoring Service (CAMS) Global anthropogenic emissions (CAMS-GLOB-ANT) v5.3 of 2020 (Soulie et al., 2023), the regional European CAMS anthropogenic emission inventory (CAMS-REG-ANT) v5.1 of 2020 (Kuenen et al., 2022) and the Dutch official registered emissions of $NH_3$ in 2020 (https://data.emissieregistratie.nl/export) (see Table 1). HTAP v3 has been developed by integrating official inventories over specific areas including CAMS-REG-ANT v5.1 for Europe with the EDGAR v6.1 inventory for the remaining world regions with the spatial resolution of 0.1°× 0.1°. CAMS-GLOB-ANT combines the EDGAR annual emissions and the Copernicus Atmosphere Monitoring Service TEMPOral profiles (CAMS-TEMPO) on a global scale (Guevara et al., 2021). The emissions of the most recent years are calculated based on the trends from the Community Emissions Data System (CEDS) global inventory (Hoesly et al., 2018). The resolution of CAMS-GLOB-ANT is 0.1°× 0.1°. CAMS-REG-ANT v5.1 provide yearly emissions on the spatial resolution of 0.1°× 0.05°. We have applied the regional European CAMS-TEMPO profiles (Guevara et al., 2021) to CAMS-REG-ANT v5.1 to get the monthly emissions (hereinafter referred to as CAMS-REG-TEMPO). The Dutch registered $NH_3$ emissions are taken from https://www.emissieregistratie.nl and provided annually on a high resolution of 1 km ×1 km. To compare the derived $NH_3$ emissions of DECSO spatially with bottom-up inventories, we aggregate emissions from these bottom-up inventories into the 0.2° × 0.2° grid cells of the DECSO working domain.

*Table 1. Summary of the bottom-up inventories compared to the satellite-derived $NH_3$ emissions from DECSO.*

| **Emission inventory** | **Year** | **Spatial Resolution** | **Temporal resolution** |
|---|---|---|---|
| LRTAP | 2020 | Country total | Annual |
| E-PRTR | 2020 | Point source | Annual |
| HTAP v3 | 2018 | 0.1°× 0.1° | Monthly |
| CAMS-GLOB-ANT v5.3 | 2020 | 0.1°× 0.1° | Monthly |
| CAMS-REG-ANT v5.1 | 2020 | 0.1°× 0.05° | Annual, monthly (with CAMS-REG-TEMPO) |

| | | | |
|---|---|---|---|
| Dutch Registered $NH_3$ emissions | 2020 | 1 km ×1 km | Annual |

## 2.4 DECSO

DECSO is an inversion algorithm developed for the purpose of deriving emissions of short-lived species from satellite observations. As such DECSO has been specifically designed to use daily satellite observations of column concentrations to provide rapid updates of emission estimates of short-lived atmospheric constituents on a regional scale. An extended Kalman filter is used, in which emissions are translated to column concentrations via the CTM and these are compared to the satellite column observations. Based on that single forward CTM simulation, the sensitivity of concentrations to emissions is calculated by using trajectory analyses to account for transport away from the source. In previous studies, DECSO has been applied to $NO_2$ observations from different satellites including TROPOMI to estimate $NO_x$ emissions (Mijling et al., 2013; Ding et al., 2015; van der A et al., 2020; Ding et al., 2022; Ding et al., 2020; van der A et al., 2024). The studies revealed that the temporal and spatial variability of total surface $NO_x$ emissions are captured well by DECSO (Ding et al., 2017b; van der A et al., 2017; Liu et al., 2018; van der A et al., 2024). Here we have used the updated version DECSO v6.3 (van der A et al., 2024) for estimating simultaneously $NO_x$ and $NH_3$ emissions using the daily observations from TROPOMI and CrIS (referred to as multi-species DECSO). The main changes of v6.3 include improving the sensitivity matrix calculation and using the latest Eulerian regional off-line CTM CHIMERE v2020v3 (Menut et al., 2021) instead of CHIMERE v2013. In the CTM, we employ the Copernicus Landcover 2019 data (Buchhorn et al., 2020) , and the source sector distributions of emissions obtained from HTAP v3 of 2018, which are also used as input emissions of other species beside $NO_x$ and $NH_3$. CHIMERE is driven by the operational meteorological forecast of the European Centre for Medium-Range Weather Forecasts (ECMWF). Here we present the specific setting in DECSO for $NH_3$ (referred to as DECSO-NH3).

To update $NH_3$ emissions based on the Kalman filter equations, one of the essential calculations is the Kalman gain matrix (**K**) using the following equation:

$$\mathbf{K} = \mathbf{P}^{\mathrm{f}}(t)\mathbf{H}[\mathbf{H}\mathbf{P}^{\mathrm{f}}(t)\mathbf{H}^{\mathrm{T}} + \mathbf{R}]^{-1} \qquad (1)$$

$\mathbf{P}^{\mathrm{f}}$ is the error covariance matrix of the forecasted emissions at time *t*. **H** is the sensitivity matrix (Jacobian) describing how the $NH_3$ column concentration on a satellite footprint depends on gridded $NH_3$ emissions. **R** is the error covariance combining the observation error of tropospheric $NH_3$ columns, the uncertainty of the CTM, and representation error introduced by projection of modelled columns on the satellite footprint.

$\mathbf{P}^f$ is parametrised based on an evaluation of the emission forecast error $q$, which is the error increase during one time step of the forecast model. The emission forecast model is persistence, predicting that the emission is equal to the analysis of the emissions from the previous day. We parametrize $q$ of $NH_3$ following:

$$q = \varepsilon_{abs} \exp\left(-\frac{\varepsilon_{rel}}{\varepsilon_{abs}} e\right) + \varepsilon_{rel} e \qquad (2)$$

$\varepsilon_{abs}$ and $\varepsilon_{rel}$ are the absolute and relative errors that are the dominating emission errors for low and high emissions respectively.

To determine $\varepsilon_{abs}$, $\varepsilon_{rel}$ and also the covariance matrix **R** for $NH_3$, we follow the method described by Ding et al. (2017a) based on the analysis of Observation minus Forecast (OmF) and Observation minus Assimilation (OmA). The fitted $\varepsilon_{abs}$, $\varepsilon_{rel}$ are $0.075 \times 10^{15}$ molecule $cm^{-2}$ $h^{-1}$ and 0.045. Note that **R** is the variance of the observation error, the CTM model error and the representation error. Our analyses showed that the **R** values are dominated by the satellite observation errors ($\sigma_{obs}$). The representation error can be neglected. We set the small contribution of model errors in **R** to $0.5 \times 10^{15}$ molecule $cm^{-2}$. To capture the quick changes of $NH_3$ emissions during the fertilizing seasons and give more weight to satellite observations with high values during the assimilation, we need to reduce their high observation errors for high values and keep the same observation errors for low values. By fitting $NH_3$ observation errors ($\sigma_{obs}$) against the observed columns $C$ using all observations in 2020, we find a linear relation:

$$\bar{\sigma}_{obs} = \alpha C + b \qquad (3)$$

$\alpha$ is equal to 0.2 and $b$ is equal to $1 \times 10^{15}$ molecule $cm^{-2}$. If the given $\sigma_{obs}$ is larger than $\alpha C + b$, we use Eq (3) for the observation error in **R**.

We update $NH_3$ emissions only over land since there are~~is~~ almost no $NH_3$ emissions over oceans and seas.

As we mentioned, $NH_3$ reacts with sulfuric and nitric acids from $SO_2$ and $NO_x$ to form ~~PM2.5~~$PM_{2.5}$. The changes in $NO_x$ and $SO_2$ emissions will affect the concentration and removal of $NH_3$ in the atmosphere. Inaccurate emissions of $NO_x$ and $SO_2$ will therefore affect the inversion of $NH_3$ emissions (Kuttippurath et al., 2024). To assess the sensitivity of $NH_3$ emissions derived with DECSO on $NO_x$ and $SO_2$ emissions, we have run DECSO with different $NO_x$ and $SO_2$ emissions (default emissions of HTAP v3 and doubling the emissions of HTAP v3 for $SO_2$ and $NO_x$) as input for the CTM. The results shows that the inversion of $NH_3$ emissions is not sensitive to the change of $SO_2$ emissions, but it is to $NO_x$ emissions. In Europe, the impact of $SO_2$ emissions on $NH_3$ can be neglected nowadays due to the low $SO_2$ emissions (Luo et al., 2022), which have been reduced by 80% in 2020 compared to 2005 (EEA, 2023). The sensitivity tests indicate that up-to-date $NO_x$ emissions are very important for the accurate inversion of $NH_3$ emissions. The monthly $NO_x$ emissions of HTAP in 2018 and derived with DECSO in 2020 are quite different over the various countries (Figure S3). In 2020, due to the COVID-

19 pandemic, $NO_x$ emissions reduced compared to other years. van der A et al. (2024) has compared the seasonality of $NO_x$ emissions of DECSO to other bottom-up inventories and showed individual temporal variability of industrial facilities is derived with DECSO in Europe, while bottom-up inventories use the same temporal profile per country per sector and no detailed information of the temporal changes of individual sources. We estimate $NH_3$ and $NO_x$ emissions with DECSO simultaneously (the multi-specie DECSO) from CrIS and TROPOMI on a daily basis. We use the DECSO-NH3 version to estimate only $NH_3$ emissions from CrIS and use $NO_x$ emissions of HTAP v3 as input for the CTM. Figure 1 shows the difference of monthly $NH_3$ emissions in three countries (Netherlands, Italy and Greece) derived with the multi-species DECSO version and the DECSO-NH3 version. The derived $NH_3$ emissions all differ largely (up to ±40%) in winter and less in summer.

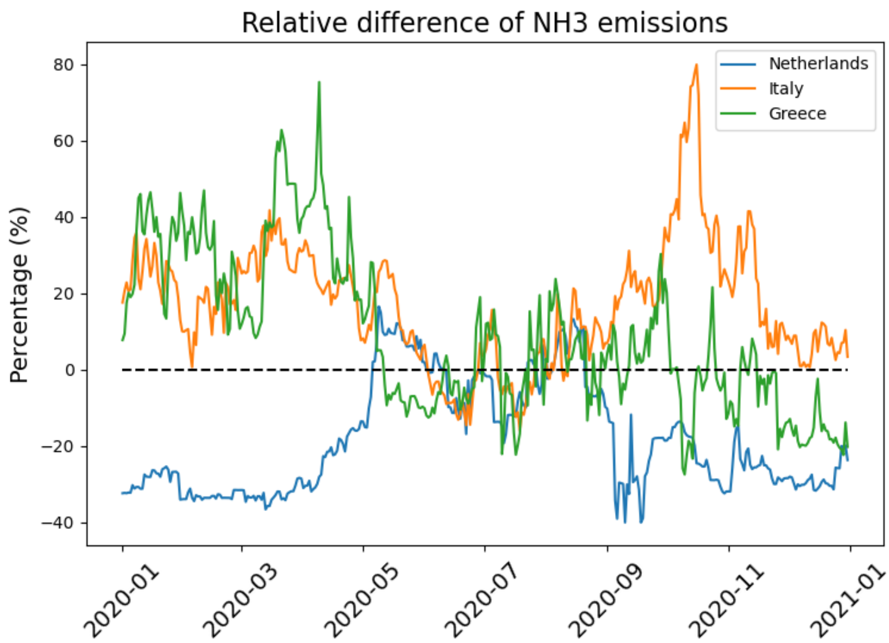


*Figure 1. The relative difference (multi-species DECSO minus DECSO-NH3) of $NH_3$ emissions between multi-species DECSO and DECSO-NH3. DECSO-NH3 means that only $NH_3$ emissions are derived with CrIS-NOAA-20. multi-species DECSO means that $NH_3$ and $NO_x$ emissions are derived using CrIS-NOAA-20 and TROPOMI observations.*

## 3. Results

### 3.1 $NH_3$ emissions in Europe

We have run the multi-species DECSO ~~parallel~~ version with $NH_3$ observations from CrIS-NOAA-20 and CrIS-SNPP respectively to estimate $NH_3$ emissions over the selected domain of Europe in 2020 (Figure 2~~Figure 2~~), ~~.~~ which is the only year with a full year overlap of $NH_3$ observations for these two satellites. The total $NH_3$ emissions over the study domain are 8.0 Tg/year from SNPP and 8.1 Tg /year from NOAA-20. The spatial distribution of the $NH_3$ emissions derived from the two satellites agrees well, with small differences (with a relative root mean square difference of 1.2%) resulting from deviations of the observed $NH_3$ columns. The spatial distribution of high $NH_3$ emissions derived from DECSO is similar to that of HTAP, CAMS-REG-ANT and CAMS-GLOB-ANT but with more local-scale variability and hotspots. The total emissions of DECSO over the European domain are higher than HTAP (4.2 Tg/year), CAMS-REG-ANT (4.0 Tg/year) and CAMS-GLOB-ANT (5.9 Tg/year)

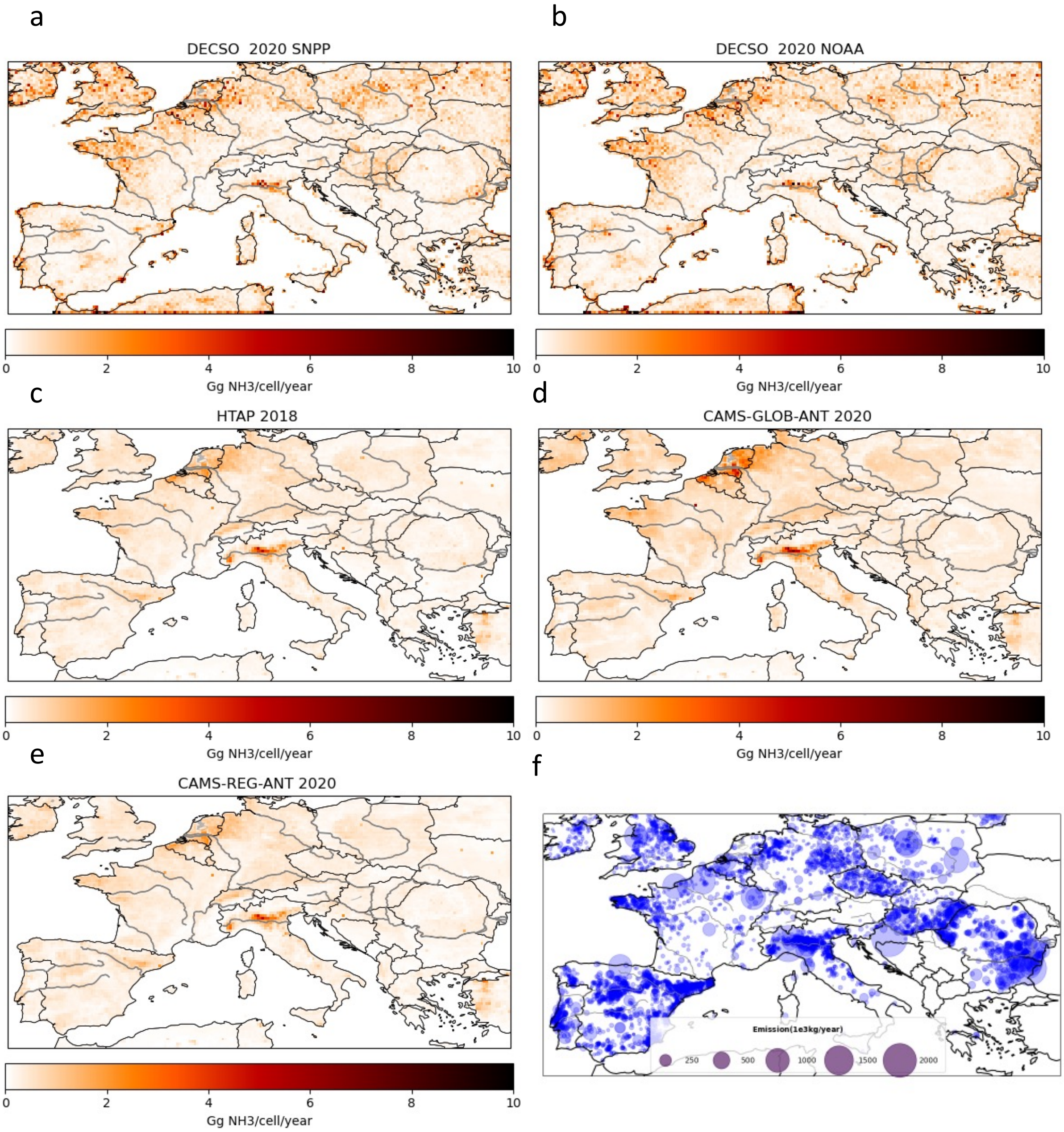


*Figure 2. $NH_3$ emission maps. $NH_3$ emissions derived with DECSO from (a) SNPP and (b) NOAA-20 in 2020. $NH_3$ emissions of (c) HTAP in 2018, (d) CAMS-GLOB-ANT in 2020 (e) CAMS-REG-ANT in 2020. (f) The registered point sources of E-PRTR in 2017.*

The locations of high $NH_3$ emissions, especially in Po-Valley, Spain, Hungary and the east of Romania, shown in DECSO are highly corelated to the registered $NH_3$ point sources of E-PRTR which are from industrial facilities including livestock facilities but not from fertilizer applications. We see that emissions from the Netherlands are high in DECSO and the bottom-up inventories but are missing in the database of E-PRTR. For the countries in East Europe (e.g. Poland, Hungary, Romania), the $NH_3$ emissions derived with DECSO are much higher than from the bottom-up inventories. To assess the $NH_3$ emissions per country, we calculated the country total emissions (see Figure 3~~Figure 3~~). The correlation coefficients of country totals from DECSO with the bottom-up inventories are all higher than 0.95. In general, the country totals of $NH_3$ emissions derived by DECSO from either NOAA-20 or SNPP are comparable to HTAP, LRTAP, CAMS-REG-ANT and CAMS-GLOB-ANT, with DECSO about 30% higher. HTAP, LRTAP and CAMS-REG-ANT have very similar emissions per country, while CAMS-GLOB-ANT shows higher emissions than the other three bottom-up inventories. Because HTAP v3 uses annual emissions from CAMS-REG-ANT for Europe, the only difference between HTAP v3 and CAMS-REG-ANT is the difference in year. The input of CAMS-REG-ANT is mainly based on LRTAP. CAMS-GLOB-ANT is based on EDGAR and use different emission activities and factors compared to the other three bottom-up inventories. In the North part of Europe, for example Netherlands and Germany, DECSO results show lower $NH_3$ emissions than CAMS-GLOB-ANT but higher than HTAP, LRTAP and CAMS-REG-ANT.

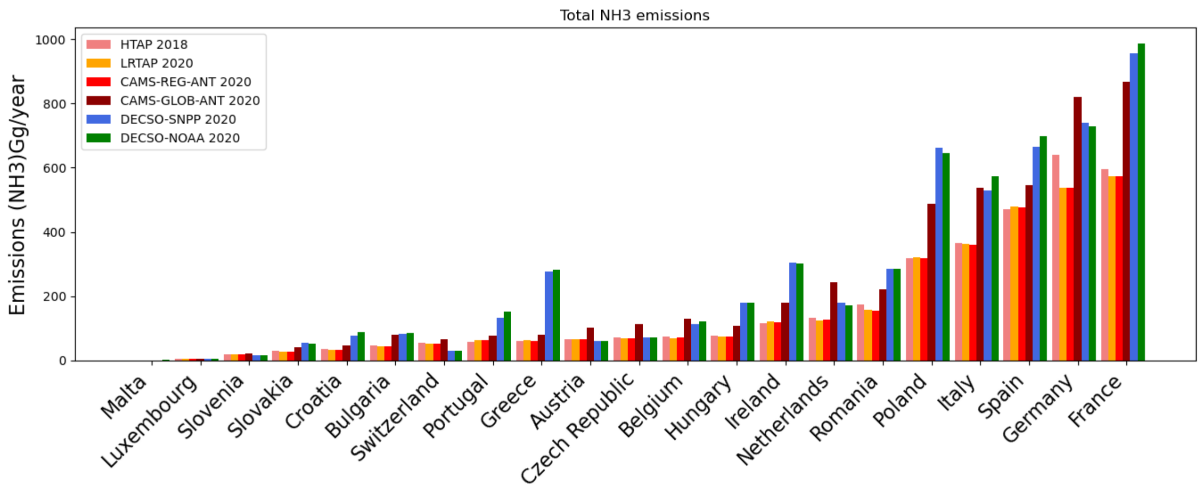


*Figure 3 Country totals of $NH_3$ emissions (Gg/year) according to database LRTAP in 2020~~18~~, bottom-up inventories HTAP in 2018, CAMS-REG-ANT in 2020, CAMS-GLOB-ANT in 2020 and the DECSO calculations from SNPP and NOAA-20 in 2020.*

To analyze the seasonality of $NH_3$ emissions derived from DECSO, we compare the monthly emissions of DECSO with bottom-up inventories. Figure 4~~Figure 4~~ shows the monthly $NH_3$ emissions from DECSO, HTAP, CAMS-REG-TEMPO, and CAMS-GLOB-ANT of the Netherlands, Spain, France and

Poland. We see that the seasonal cycle of $NH_3$ emissions of DECSO is~~are~~ closer to CAMS-GLOB-ANT. HTAP shows the exact same monthly variability for each country. CAMS-REG-TEMPO shows very similar monthly patterns to the ones reported by CAMS-GLOB-ANT as they are both using the same method to derive the temporal profiles for livestock and agricultural soil emissions (Guevara et al., 2021). In the Netherlands as an example for north Europe, the monthly $NH_3$ emissions of DECSO are lower than CAMS-GLOB-ANT but very close to CAMS-REG-ANT. Two peaks of $NH_3$ emissions show up in April and August for CAMS emissions. This is also confirmed by the monthly surface concentrations measured by the MAN network (Figure S4). In Spain and France, the monthly emissions of DECSO are comparable to CAMS-GLOB-ANT. In the east part of Europe, such as Poland, DECSO estimates higher emissions. Note that in s~~S~~pring, when the $NH_3$ emissions are high due to fertilizer applications on farms, the $NH_3$ emissions derived with DECSO can suffer from a time lag due to insufficient observations (e.g. due to cloudiness, see Figure S5).

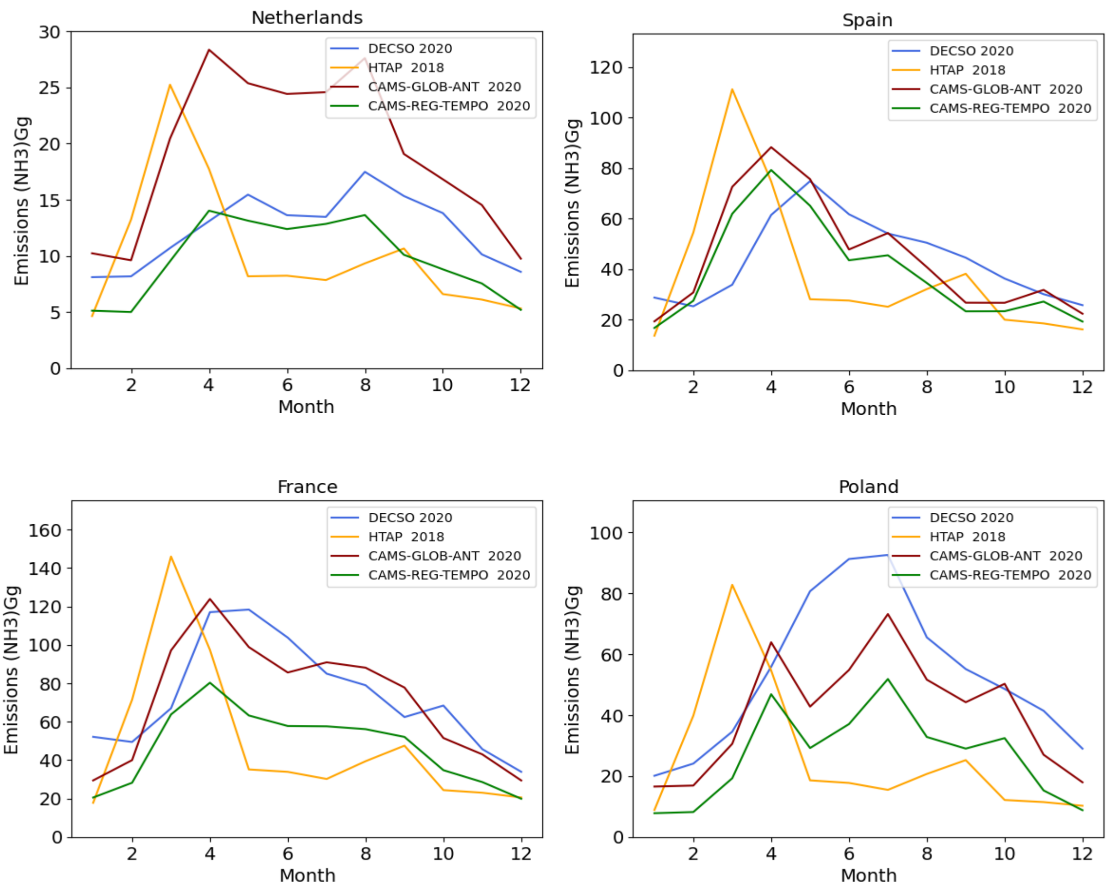


*Figure 4 Monthly $NH_3$ emissions (Gg/month) of DECSO in 2020, HTAP in 2018, CAMS-REG-TEMPO in 2020 and CAMS-GLOB-TEMPO in 2020 for (a) the Netherlands, (b) Spain, (c) France and (d) Poland.*

3.2 Emissions in the Netherlands

On the emission maps of Figure 2~~Figure 2~~, we see that the Netherlands and Po-valley have the highest emission intensity of $NH_3$. In this section, we focus our analysis on the Netherlands since it has the densest network for monitoring surface $NH_3$ concentrations and also a detailed emission inventory on a very high spatial resolution. The total emissions of the Netherlands estimated from the two satellites are very similar (Figure 3), but the spatial distributions show significant differences (Figure S6). One possible reason is that about 10% more observations are available from NOAA-20 than SNPP in 2020 (see Figure S7). The number of valid observations is in general low at high latitudes (Figure S8). More observations allow the detection of fast changes of $NH_3$ emissions from day to day. By averaging the emissions, the information from both satellites is combined and improved the quality of the derived emissions due to a doubling of the number of observations. We use the average of the results of DECSO-SNPP and DECSO-NOAA-20 to get a better spatial distribution of $NH_3$ emissions derived from satellite observations.

We compare the total $NH_3$ emissions of DECSO with CAMS-GLOB-ANT, HTAP and official national $NH_3$ emissions of the Netherlands, which are 148, 230, 122 and 123 Gg/year respectively. DECSO is lower than CAMS-GLOB-ANT but higher than HTAP and the official $NH_3$ emissions of the Netherlands. Figure 5~~Figure 5~~ shows the spatial distribution of each inventory in the Netherlands. We see that DECSO captures the high emission areas and regional distribution over the country. The correlation coefficients of the spatial distribution of $NH_3$ emissions between DECSO and the national emissions of the Netherlands, HTAP v3, CAMS-GLOB-ANT are 0.87, 0.87 and 0.88 respectively. At the resolution of the individual DECSO grid cells, 0.2° × 0.2° grid cell, the emission patterns show differences. This may be due to uncertainties in the location of the emissions and displacements by up to ~~0.5° to 1°~~one grid cell, similar as for $NO_x$ emissions (van der A et al., 2024). For example, the emission sources at the edge of grid cells can be spread to the neighbouring grid cells.

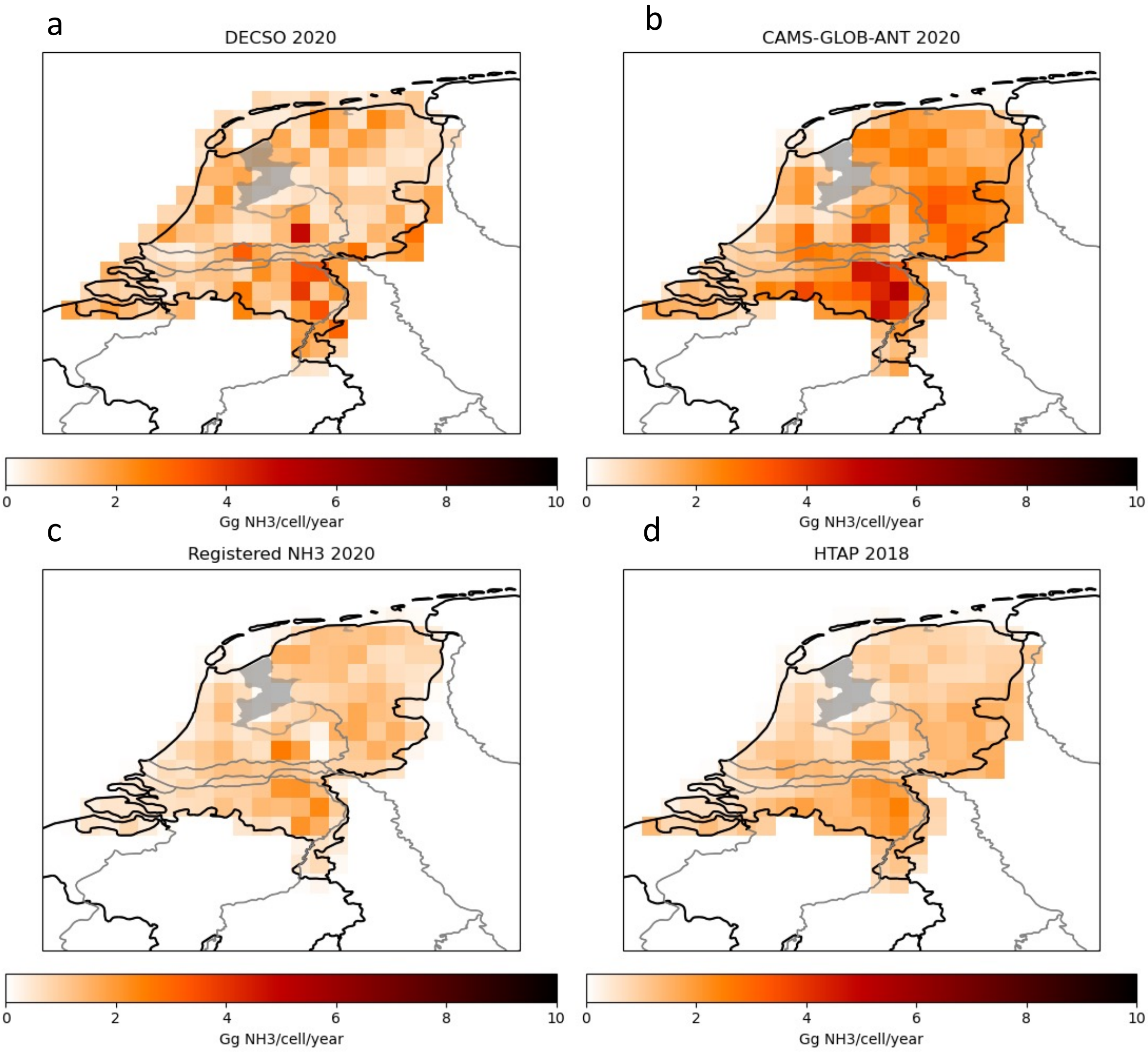


*Figure 5 $NH_3$ emissions in the Netherlands. (a) The averaged $NH_3$ emissions derived with DECSO from SNPP and NOAA-20. (b) $NH_3$ emissions of CAMS-GLOB-ANT in 2020. (c) The official national $NH_3$ emissions for the Netherlands in 2020 (from emissieregistratie.nl). (d) $NH_3$ emissions of HTAP in 2018.*

To further assess the DECSO results using in-situ observations from both LML and MAN networks in the Netherlands, we have conducted three runs of CHIMERE for the year 2020 using $NH_3$ emissions from DECSO in 2020, HTAP in 2018 and CAMS-GLOB-ANT in 2020 over the European domain (same as the setup of DECSO). To compare to the surface $NH_3$ measurement from the MAN network, we calculate the monthly average of surface $NH_3$ concentrations from the model simulations. Figure 6 (a-c) shows the scatter plots of monthly $NH_3$ concentrations of model simulations against observations for the whole year. We see that modelled $NH_3$ concentrations with the HTAP emissions are underestimated and those with the CAMS-GLOB-ANT emissions are overestimated compared to in-situ observations. The modelled $NH_3$ concentrations with DECSO emissions have the lowest absolute bias (modelled concentration minus in-situ observations of the MAN network) (Figure 7). The performance of model simulations is better in summer months (April to September) than in winter months (October-March). In winter months, few cloud-free satellite observations are available for the Netherlands. For DECSO, the scatter plot looks more spread out than in summer months (Figure 6d-i). In summer months, the $NH_3$ concentrations with CAMS-GLOB-ANT are largely overestimated and with HTAP are largely underestimated, while DECSO has a lower bias compared to the other two. Note that in the grid cells, the number of stations can vary from 1 to 16. If we select grid cells with more than 3 sites, DECSO shows better spatial correlation with in-situ observations than for the other two inventories and the lowest bias (Figure 7 and Table 2).

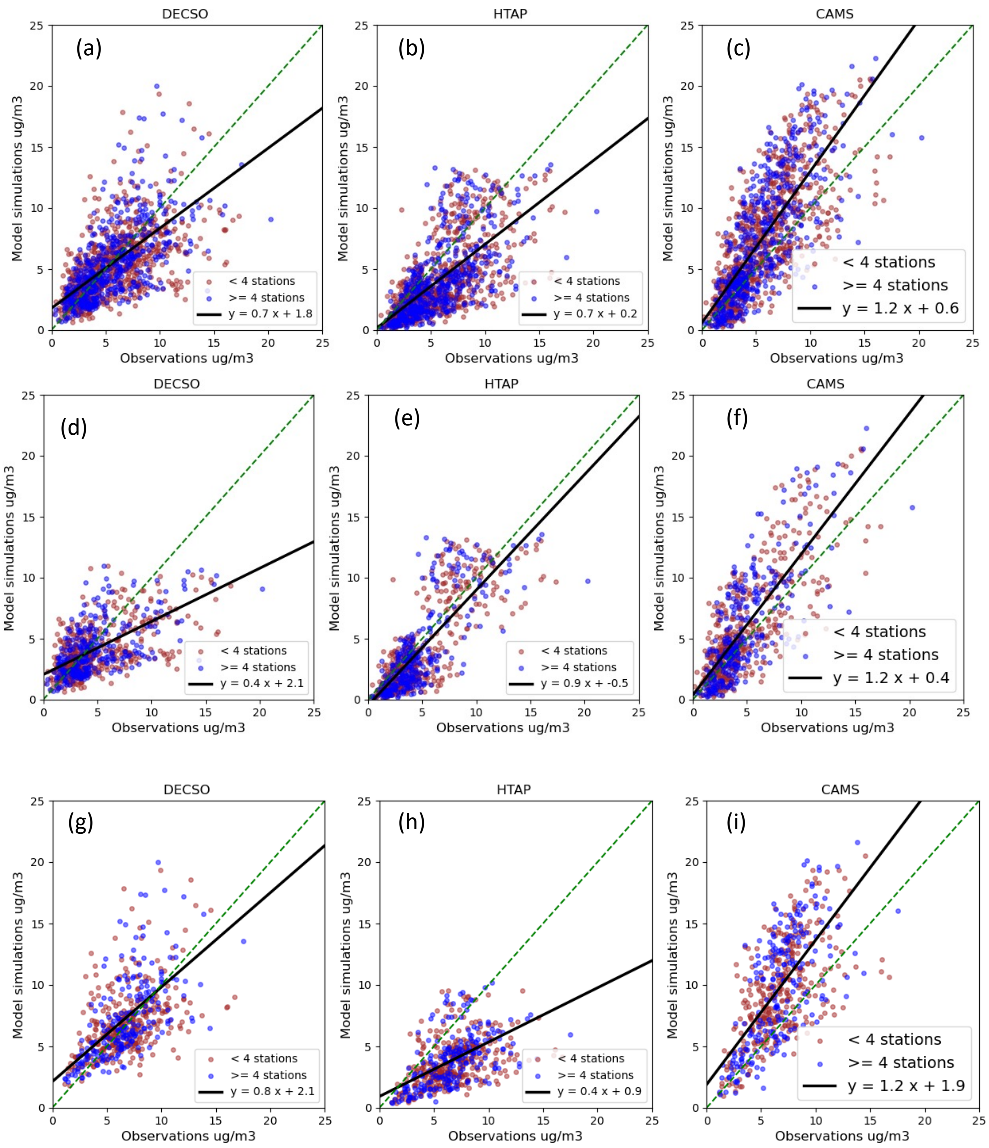


*Figure 6. Scatter plots of observations from the MAN network with $NH_3$ surface concentrations from model simulations with $NH_3$ emissions from DECSO (left column), HTAP (middle column) and CAMS-GLOB-ANT (right column). (a-c) The scatter plot of data for the whole year for all sites. (d-f) The scatter plot of the data in winter months (October to March). (g-i) The scatter plot of the data in summer months (April to September). Each point presents the model grid cells having the in-situ*

*observations. The red dots mean there are less than four in-situ sites in the grid cells. The blue dots mean there are at least four in-situ sites in the grid cell. The fitted black line is for grid cells with at least four in-situ sites.*

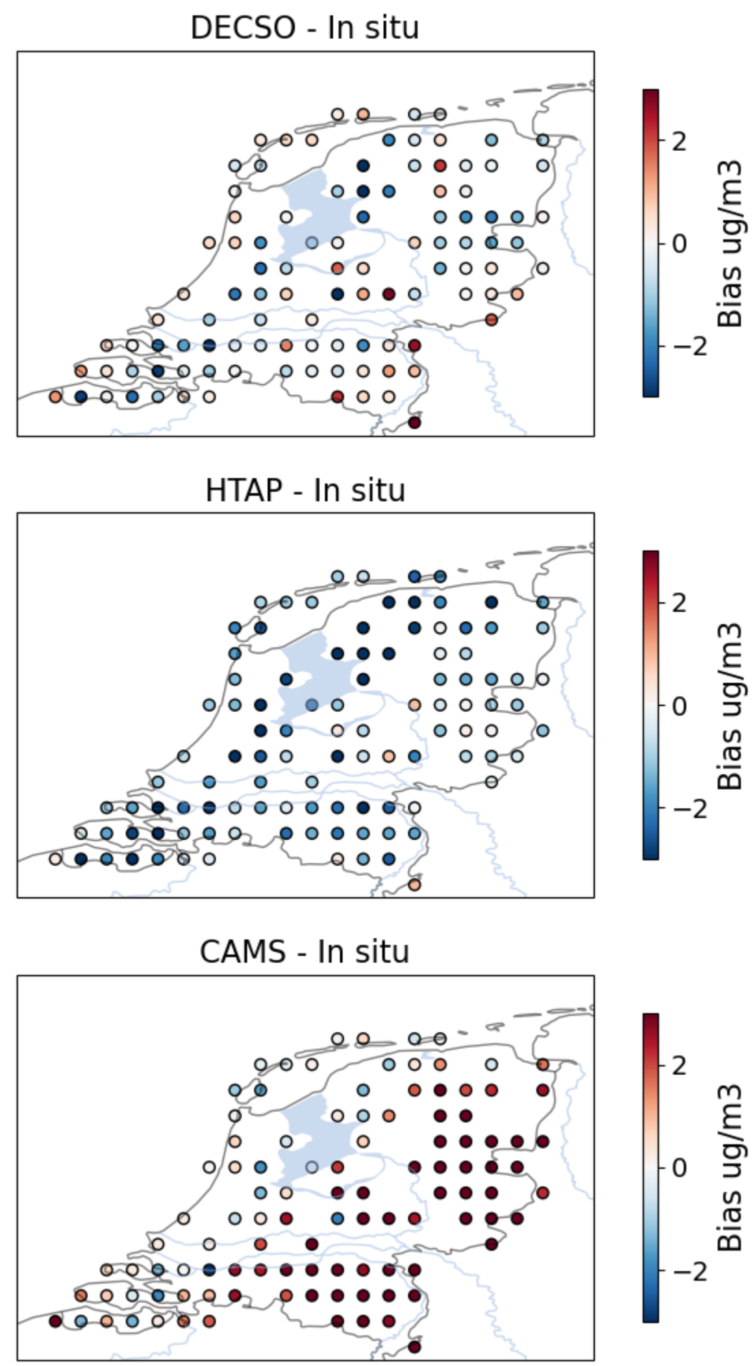


*Figure 7. Bias of the model simulated surface concentrations with $NH_3$ emissions from DECSO (left column), HTAP (middle column) and CAMS-GLOB-ANT (right column) compared to the in-situ observations from the MAN network.*

*Table 2. The spatial and temporal correlation coefficients and the bias of monthly mean simulated $NH_3$ surface concentration using DECSO, HTAP and CAMS-GLOB-ANT $NH_3$ emissions against observations of the MAN network for grid cells with more than three measurement locations.*

| | Temporal correlation coefficient | Spatial correlation coefficient | Bias (ug/m$^3$) | RMSE (ug/m$^3$) |
|---|---|---|---|---|
| DECSO | 0.64 | 0.73 | -0.2 | 2.6 |
| HTAP v3 | 0.70 | 0.70 | -1.9 | 3.0 |
| CAMS-GLOB-ANT | 0.82 | 0.70 | -0.3 | 3.8 |

The LML network has six sites measuring surface $NH_3$ concentrations, which are provided every hour. Since the difference in our model simulations is only due to the monthly input emissions of $NH_3$, we calculate monthly average $NH_3$ observations for the six sites to compare with the modelled monthly averaged concentrations. The comparison shows that the model simulations using the DECSO $NH_3$ emissions have similar performance as bottom-up inventories (Figure S9 and S10). The correlations of modelled monthly $NH_3$ concentration using DECSO and CAMS-GLOB-ANT emissions with the observations from the LML network are better than that of HTAP, while CAMS-GLOB-ANT has the lowest bias. Based on these six sites, the comparison shows that the model result using DECSO is very comparable with that using CAMS-GLOB-ANT.

### 3.3 Uncertainties and bias of $NH_3$ emissions

One advantage of DECSO is that a standard deviation of derived emissions is also calculated per grid cell on a daily basis according the Kalman filter equations. As described by van der A et al. (2024), the derived errors in the emissions are correlated in time linked to the assumption of the persistent emission forecast model. The autocorrelation effects can be neglected after about one week up to ten days. We follow the autocorrelation function presented by van der A et al. (2024) to calculate the monthly variance of $NH_3$ emissions. The monthly variance of $NH_3$ emissions for each grid cell in the study domain varies from 17% to 58%. For the Netherlands, the precision (random uncertainty) of the monthly emissions is about 20% and the precision of the annual total is about 5%.

A bias in satellite derived emissions can be introduced due to the linearisation of the averaging kernels (Sitwell et al., 2022). The CrIS ammonia observations are retrieved in logarithm space together with logarithmic averaging kernels. As discussed by Sitwell et al. (2022), either using the logarithmic averaging kernel or the linearized averaging kernel introduces a bias when applying them to the model simulated profiles. The logarithmic averaging kernels cause problems when the model profiles are zero at any point in the profile and lead to a positive bias in emission estimates. Linearized averaging kernels may introduce a negative bias in emissions when there is a large difference between the model profile and the a priori profile used in the retrieval.

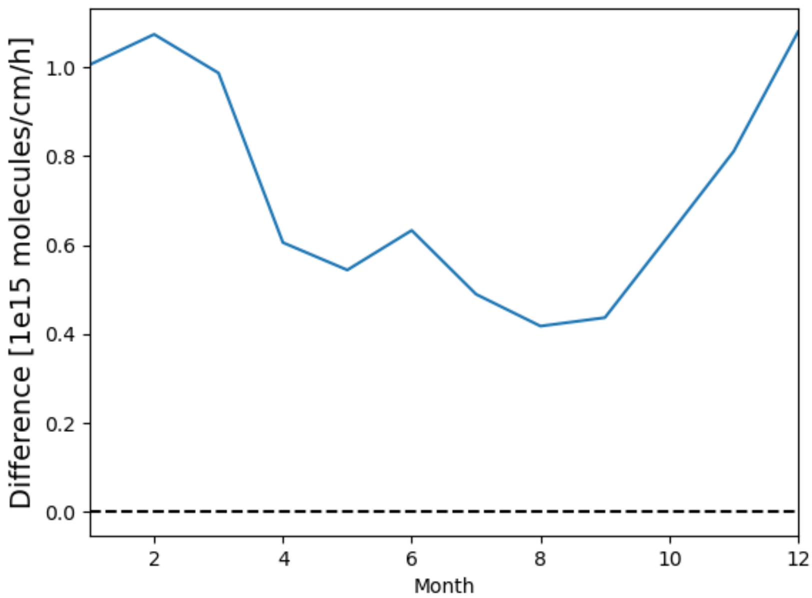


*Figure 8. The absolute change of monthly $NH_3$ emissions (molecule/cm²/h) if there is a positive bias of $5\times 10^{15}$ molecule/cm² of each $NH_3$ column observation.*

To assess how the biases in satellite $NH_3$ observations affect emissions derived by DECSO, we have done two simple bias tests. For the first test, the $NH_3$ columns of CrIS on NOAA-20 are increased by 20%, a positive relative bias for the satellite observations. The annual emissions of $NH_3$ with the introduced bias increase by 27% for the European domain. It seems that the introduced bias has a higher impact on emissions in winter than in summer. The relative bias on emissions can be as high as 50% in winter. The change of emissions in summer becomes even negative probably because $NH_3$ column concentrations can show a large variation from day to day. When the $NH_3$ columns are very high on one day and next drop to a very low value, the absolute change in concentration is larger than the original situation without introduced bias. This will lead to a larger decrease in the updated emissions and can result in a negative change of emissions. For the second test, an absolute bias of $5\times 10^{15}$ molecule/cm$^2$ is added to each $NH_3$ column observation of CrIS on NOAA-20. Figure 8 shows the increase of $NH_3$ emissions caused by the absolute bias introduced in the satellite observations. We see that the increase is doubled in winter compared to summer, because the lifetime in winter is longer than in summer. The averaged effective lifetime calculated with DECSO is about 10 hours in winter and 5 hours in summer. With the same bias of $NH_3$ columns, the impact on emissions is larger in winter than in summer.

## 4. Discussion and Conclusion~~s~~

To derive $NH_3$ emissions from satellite data, we presented an updated version of the DECSO algorithm with specific settings for $NH_3$. Together with the improved the DECSO version for $NO_x$ of van der A et al. (2024), we have the multi-species DECSO version to update $NO_x$ and $NH_3$ emissions simultaneously. In general, the removal of $NH_3$ in the atmosphere is affected by the amount of $NO_x$ and $SO_2$ emissions. For the study domain of Europe, our sensitivity study shows that the influence of changes in $NO_x$ emissions need to be considered in the inversion of $NH_3$ emissions in DECSO. The impact of $SO_2$ emissions is very small and can be neglected since the $SO_2$ emissions are usually low in Europe. Thus, to derive $NH_3$ emissions and to analyze the seasonal cycle and trend of $NH_3$ emissions from satellite observations over Europe, it is recommended to include updated $NO_x$ emissions in the inversion calculation of $NH_3$ emissions in DECSO. For regions with high $SO_2$ emissions, it is necessary to consider if the $SO_2$ emissions are changing rapidly and are up-to-date in the inversion.

The error covariances of the updated daily $NH_3$ emissions per grid cell are provided during the calculation in DECSO. Considering the autocorrelations introduced by the assumption of the persistency emission model, the calculated monthly error on $NH_3$ emissions for each grid cell in the study domain varies from 17% to 58%. The yearly error per grid cell is about 5 ~ 15%. The sensitivity tests for retrieval biases shows that with an introduced constant relative and absolute bias in $NH_3$ retrievals, the resulting bias in emissions derived with DECSO shows a seasonal variability with a peak in winter. This means the algorithm is more sensitive to a bias in the observations during wintertime.

The total $NH_3$ emissions in our European domain derived from $NH_3$ observations of SNPP and NOAA-20 are 8.0 Tg/year and 8.1 Tg/year respectively with a precision of about ~~0.2~~5 - 17 % per grid cell/year. The difference in country total emissions derived from the two satellites is very small. However, the details of the spatial distribution of emissions derived from both satellites are different over the north part of the domain, such as the Netherlands. This may be due to the varying number of observations per region per year from the two satellites. An average of the emissions derived from both satellites leads to an improved spatial distribution compared to the emissions from the individual satellite. The spatial distribution of derived $NH_3$ emissions is similar to the bottom-up inventories, but DECSO emissions are in general higher. The annual total emissions derived by DECSO for the whole domain is larger than the bottom-up inventories (LRTAP, HTAP, CAMS-REG-ANT and CAMS-GLOB-ANT). The comparison of country total emissions shows that DECSO gives higher $NH_3$ emissions for the countries in East Europe than the bottom-up inventories. In addition, DECSO results show higher sources in Spain, Hungary and the east of Romania. This is in line with the registered point sources of E-PRTR. The seasonal cycle of the emissions of DECSO are comparable to CAMS-GLOB-ANT, while HTAP uses the same seasonal cycle for each country in Europe. The analysis indicates that DECSO can be used to estimate $NH_3$ over a long period for the trend study. The retrieval product of $NH_3$ from SNPP ends in May 2021. Because of the insignificant differences in $NH_3$ emissions derived from the two satellites for the overlap year 2020, the trends analysis can be continued by using the $NH_3$ data from NOAA-20 (Figure S11. We have shown the importance of the impact of $NO_x$ emissions on the inversion of $NH_3$ emissions. Since the $NO_x$ emissions derived from TROPOMI have good agreement with CAMS-REG-ANT, as shown by van der A et al. (2024). the $NO_x$ emissions from CAMS-REG-ANT can be used for the years before 2019 in trend studies of $NH_3$ emissions over Europe.

For the Netherlands, model simulations using $NH_3$ emissions from DECSO, HTAP and CAMS-GLOB-ANT are compared to in-situ observations from the MAN and LML networks. In general, the simulation using DECSO emissions has a lower bias, but also a lower temporal correlation compared to CAM-GLOB-ANT. The performance of model simulations with DECSO is better in summer than in winter. Both the bias and spatial correlation between model simulations using DECSO emissions and the MAN in-situ observations are higher than CAMS-GLOB-ANT for grid cells including more than 3 measurement sites. We conclude that satellite-derived emissions derived with DECSO show a comparable temporal and spatial distribution as bottom-up inventories. The emissions derived from satellite observations can provide fully independent information on emissions for verifying the bottom-up inventories. With the global coverage of satellite observations, DECSO can be easily applied to different regions. After validation of DECSO over regions like Europe, where there is sufficient information of emissions, the added value of DECSO for deriving $NH_3$ emissions is to provide $NH_3$ emissions over regions with limited local information of $NH_3$ emissions.

## Data

The CrIS $NH_3$ data v1.6.4 of SNPP and NOAA-20 created by Environment and Climate Change Canada are currently publicly available upon request (mark.shephard@canada.ca) at https://hpfx.collab.science.gc.ca/~mas001/satellite_ext/cris/snpp/nh3/v1_6_4.

The TROPOMI NO2 data version 2.4 are available via the Copernicus website https://dataspace.copernicus.eu/ and via the TEMIS website https://www.temis.nl/airpollution/no2.php (last access: 02 August 2024) (https://doi.org/10.5270/S5P-9bnp8q8TS15 ).

The $NH_3$ and $NO_x$ emissions of DECSO v6.3 are available on the GlobEmission website https://www.temis.nl/emissions/data.php.

HTAP v3 dataset are available on https://edgar.jrc.ec.europa.eu/dataset_htap_v3

The European emissions data sets for countries NEC, LRTAP and large facilities E-PRTR are available on the website https://www.eea.europa.eu/en/analysis of the EEA.

The CAMS databases CAMS-REG-ANT v5.1, CAMS-GLOB-ANT, CAMS-TEMPO are available on the ECCAD website https://permalink.aeris-data.fr.

The $NH_3$ observation data from the LML network are available on the RIVM website https://data.rivm.nl/data/luchtmeetnet/.

The $NH_3$ observation data from the MAN network are available at https://man.rivm.nl.

The Dutch registered $NH_3$ emissions are available at https://data.emissieregistratie.nl/export

## Author contribution

JD developed the inversion algorithm of $NH_3$, performed all emission inversions, conducted the analysis and wrote the manuscript. RA and JD made the improvement of the inversion algorithm of NOx. HE developed the superobservation code. ED provided the code for a linearization of the averaging kernels of CrIS. MS provided the CrIS data. RWK provided the $NH_3$ observation data from the MAN and LML networks. MGV provided the CAMS-TEMPO profiles. LT provided suggestions during the research. All authors contributed to the reviewing and editing of the manuscript.

## Acknowledgments

This the work was financed by the Sentinel EO-based Emission and Deposition Service (SEEDS, Grant ID 101004318) project that has received funding from the European Union's Horizon 2020 research and innovation programme. Part of the work was funded by the Nationaal Kennisprogramma Stikstof (NKS) of the Dutch Ministry of Agriculture, Nature and Food Quality.

## References


Adams, C., McLinden, C. A., Shephard, M. W., Dickson, N., Dammers, E., Chen, J., Makar, P., Cady-Pereira, K. E., Tam, N., Kharol, S. K., Lamsal, L. N., and Krotkov, N. A.: Satellite-derived emissions of carbon monoxide, ammonia, and nitrogen dioxide from the 2016 Horse River wildfire in the Fort McMurray area, Atmos. Chem. Phys., 19, 2577-2599, 10.5194/acp-19-2577-2019, 2019.

Backes, A., Aulinger, A., Bieser, J., Matthias, V., and Quante, M.: Ammonia emissions in Europe, part I: Development of a dynamical ammonia emission inventory, Atmospheric Environment, 131, 55-66, https://doi.org/10.1016/j.atmosenv.2016.01.041, 2016a.

Backes, A. M., Aulinger, A., Bieser, J., Matthias, V., and Quante, M.: Ammonia emissions in Europe, part II: How ammonia emission abatement strategies affect secondary aerosols, Atmospheric Environment, 126, 153-161, https://doi.org/10.1016/j.atmosenv.2015.11.039, 2016b.

Beer, R., Shephard, M. W., Kulawik, S. S., Clough, S. A., Eldering, A., Bowman, K. W., Sander, S. P., Fisher, B. M., Payne, V. H., Luo, M., Osterman, G. B., and Worden, J. R.: First satellite observations of lower tropospheric ammonia and methanol, Geophysical Research Letters, 35, https://doi.org/10.1029/2008GL033642, 2008.

Behera, S. N., Sharma, M., Aneja, V. P., and Balasubramanian, R.: Ammonia in the atmosphere: a review on emission sources, atmospheric chemistry and deposition on terrestrial bodies, Environmental Science and Pollution Research, 20, 8092-8131, 10.1007/s11356-013-2051-9, 2013.

Berkhout, A. J. C., Swart, D. P. J., Volten, H., Gast, L. F. L., Haaima, M., Verboom, H., Stefess, G., Hafkenscheid, T., and Hoogerbrugge, R.: Replacing the AMOR with the miniDOAS in the ammonia monitoring network in the Netherlands, Atmos. Meas. Tech., 10, 4099-4120, 10.5194/amt-10-4099-2017, 2017.

Beusen, A. H. W., Bouwman, A. F., Heuberger, P. S. C., Van Drecht, G., and Van Der Hoek, K. W.: Bottom-up uncertainty estimates of global ammonia emissions from global agricultural production systems, Atmospheric Environment, 42, 6067-6077, https://doi.org/10.1016/j.atmosenv.2008.03.044, 2008.

Boersma, K. F., Vinken, G. C. M., and Eskes, H. J.: Representativeness errors in comparing chemistry transport and chemistry climate models with satellite UV–Vis tropospheric column retrievals, Geosci. Model Dev., 9, 875-898, 10.5194/gmd-9-875-2016, 2016.

Buchhorn, M., Smets, B., Bertels, L., De Roo, B., Lesiv, M., Tsendbazar, N.-E., Herold, M., and Fritz, S.: Copernicus Global Land Service: Land Cover 100m: collection 3: epoch 2019: Globe, 10.5281/zenodo.3939050, 2020.

Cao, H., Henze, D. K., Shephard, M. W., Dammers, E., Cady-Pereira, K., Alvarado, M., Lonsdale, C., Luo, G., Yu, F., Zhu, L., Danielson, C. G., and Edgerton, E. S.: Inverse modeling of NH3 sources using CrIS remote sensing measurements, Environmental Research Letters, 15, 104082, 10.1088/1748-9326/abb5cc, 2020.

Cao, H., Henze, D. K., Zhu, L., Shephard, M. W., Cady-Pereira, K., Dammers, E., Sitwell, M., Heath, N., Lonsdale, C., Bash, J. O., Miyazaki, K., Flechard, C., Fauvel, Y., Kruit, R. W., Feigenspan, S., Brümmer, C., Schrader, F., Twigg, M. M., Leeson, S., Tang, Y. S., Stephens, A. C. M., Braban, C., Vincent, K., Meier, M., Seitler, E., Geels, C., Ellermann, T., Sanocka, A., and Capps, S. L.: 4D-Var Inversion of European NH3 Emissions Using CrIS NH3 Measurements and GEOS-Chem Adjoint With Bi-Directional and Uni-Directional Flux Schemes, Journal of Geophysical Research: Atmospheres, 127, e2021JD035687, https://doi.org/10.1029/2021JD035687, 2022.

Chen, Y., Shen, H., Kaiser, J., Hu, Y., Capps, S. L., Zhao, S., Hakami, A., Shih, J. S., Pavur, G. K., Turner, M. D., Henze, D. K., Resler, J., Nenes, A., Napelenok, S. L., Bash, J. O., Fahey, K. M., Carmichael, G. R., Chai, T., Clarisse, L., Coheur, P. F., Van Damme, M., and Russell, A. G.: High-resolution hybrid inversion of IASI ammonia columns to constrain US ammonia emissions using the CMAQ adjoint model, Atmos. Chem. Phys., 21, 2067-2082, 10.5194/acp-21-2067-2021, 2021.

Clarisse, L., Clerbaux, C., Dentener, F., Hurtmans, D., and Coheur, P.-F.: Global ammonia distribution derived from infrared satellite observations, Nature Geoscience, 2, 479-483, 10.1038/ngeo551, 2009.

Crippa, M., Guizzardi, D., Muntean, M., Schaaf, E., Dentener, F., van Aardenne, J. A., Monni, S., Doering, U., Olivier, J. G. J., Pagliari, V., and Janssens-Maenhout, G.: Gridded emissions of air pollutants for the period 1970–2012 within EDGAR v4.3.2, Earth Syst. Sci. Data, 10, 1987-2013, 10.5194/essd-10-1987-2018, 2018.

Crippa, M., Guizzardi, D., Butler, T., Keating, T., Wu, R., Kaminski, J., Kuenen, J., Kurokawa, J., Chatani, S., Morikawa, T., Pouliot, G., Racine, J., Moran, M. D., Klimont, Z., Manseau, P. M., Mashayekhi, R., Henderson, B. H., Smith, S. J., Suchyta, H., Muntean, M., Solazzo, E., Banja, M., Schaaf, E., Pagani, F., Woo, J. H., Kim, J., Monforti-Ferrario, F., Pisoni, E., Zhang, J., Niemi, D., Sassi, M., Ansari, T., and Foley, K.: The HTAP_v3 emission mosaic: merging regional and global monthly emissions (2000–2018) to support air quality modelling and policies, Earth Syst. Sci. Data, 15, 2667-2694, 10.5194/essd-15-2667-2023, 2023.

Dammers, E., McLinden, C. A., Griffin, D., Shephard, M. W., Van Der Graaf, S., Lutsch, E., Schaap, M., Gainairu-Matz, Y., Fioletov, V., Van Damme, M., Whitburn, S., Clarisse, L., Cady-Pereira, K., Clerbaux, C., Coheur, P. F., and Erisman, J. W.: NH3 emissions from large point sources derived from CrIS and IASI satellite observations, Atmos. Chem. Phys., 19, 12261-12293, 10.5194/acp-19-12261-2019, 2019.

Ding, J., van der A, R. J., Mijling, B., and Levelt, P. F.: Space-based NOx emission estimates over remote regions improved in DECSO, Atmos. Meas. Tech., 10, 925-938, 10.5194/amt-10-925-2017, 2017a.

Ding, J., van der A, R. J., Mijling, B., Levelt, P. F., and Hao, N.: NOx emission estimates during the 2014 Youth Olympic Games in Nanjing, Atmos. Chem. Phys., 15, 9399-9412, 10.5194/acp-15-9399-2015, 2015.

Ding, J., van der A, R., Mijling, B., de Laat, J., Eskes, H., and Boersma, K. F.: NOx emissions in India derived from OMI satellite observations, Atmospheric Environment: X, 14, 100174, https://doi.org/10.1016/j.aeaoa.2022.100174, 2022.

Ding, J., van der A, R. J., Eskes, H. J., Mijling, B., Stavrakou, T., van Geffen, J. H. G. M., and Veefkind, J. P.: NOx Emissions Reduction and Rebound in China Due to the COVID-19 Crisis, Geophysical Research Letters, 47, e2020GL089912, 10.1029/2020GL089912, 2020.

Ding, J., Miyazaki, K., van der A, R. J., Mijling, B., Kurokawa, J. I., Cho, S., Janssens-Maenhout, G., Zhang, Q., Liu, F., and Levelt, P. F.: Intercomparison of NOx emission inventories over East Asia, Atmos. Chem. Phys., 17, 10125-10141, 10.5194/acp-17-10125-2017, 2017b.

EEA: Emissions of the main air pollutants in Europe, https://www.eea.europa.eu/en/analysis/indicators/emissions-of-the-main-air?activeAccordion=ecdb3bcf-bbe9-4978-b5cf-0b136399d9f8, last access: 3 April, 2024.

EPRTR: European Pollutant Release and Transfer Register, database version v4.2 [dataset], http://prtr.ec.europa.eu/,2012.

Erisman, J. W., Sutton, M. A., Galloway, J., Klimont, Z., and Winiwarter, W.: How a century of ammonia synthesis changed the world, Nature Geoscience, 1, 636-639, 10.1038/ngeo325, 2008.

Erisman, J. W., Galloway, J. N., Seitzinger, S., Bleeker, A., Dise, N. B., Petrescu, A. M. R., Leach, A. M., and de Vries, W.: Consequences of human modification of the global nitrogen cycle, Philosophical Transactions of the Royal Society B: Biological Sciences, 368, 20130116, doi:10.1098/rstb.2013.0116, 2013.

Eskes, H. J. and Eichmann, K.-U.: S5P Mission Performance Centre Nitrogen Dioxide [L2__NO2___] Readme, Tech.rep., ESA, https: //sentinel.esa.int/documents/247904/3541451/Sentinel-5P-Nitrogen-Dioxide-Level-2-Product-Readme-File, 2022.

Galloway, J. N., Townsend, A. R., Erisman, J. W., Bekunda, M., Cai, Z., Freney, J. R., Martinelli, L. A., Seitzinger, S. P., and Sutton, M. A.: Transformation of the Nitrogen Cycle: Recent Trends, Questions, and Potential Solutions, Science, 320, 889-892, doi:10.1126/science.1136674, 2008.

Ge, X., Schaap, M., Kranenburg, R., Segers, A., Reinds, G. J., Kros, H., and de Vries, W.: Modeling atmospheric ammonia using agricultural emissions with improved spatial variability and temporal dynamics, Atmos. Chem. Phys., 20, 16055-16087, 10.5194/acp-20-16055-2020, 2020.

Gu, B., Zhang, L., Van Dingenen, R., Vieno, M., Van Grinsven, H. J., Zhang, X., Zhang, S., Chen, Y., Wang, S., Ren, C., Rao, S., Holland, M., Winiwarter, W., Chen, D., Xu, J., and Sutton, M. A.: Abating ammonia is more cost-effective than nitrogen oxides for mitigating PM<sub>2.5</sub> air pollution, Science, 374, 758-762, doi:10.1126/science.abf8623, 2021.

Guevara, M., Jorba, O., Tena, C., Denier van der Gon, H., Kuenen, J., Elguindi, N., Darras, S., Granier, C., and Pérez García-Pando, C.: Copernicus Atmosphere Monitoring Service TEMPOral profiles (CAMS-TEMPO): global and European emission temporal profile maps for atmospheric chemistry modelling, Earth Syst. Sci. Data, 13, 367-404, 10.5194/essd-13-367-2021, 2021.

Han, Y., Revercomb, H., Cromp, M., Gu, D., Johnson, D., Mooney, D., Scott, D., Strow, L., Bingham, G., Borg, L., Chen, Y., DeSlover, D., Esplin, M., Hagan, D., Jin, X., Knuteson, R., Motteler, H., Predina, J., Suwinski, L., Taylor, J., Tobin, D., Tremblay, D., Wang, C., Wang, L., Wang, L., and Zavyalov, V.: Suomi NPP CrIS measurements, sensor data record algorithm, calibration and validation activities, and record data quality, Journal of Geophysical Research: Atmospheres, 118, 12,734-712,748, https://doi.org/10.1002/2013JD020344, 2013.

Hoesly, R. M., Smith, S. J., Feng, L., Klimont, Z., Janssens-Maenhout, G., Pitkanen, T., Seibert, J. J., Vu, L., Andres, R. J., Bolt, R. M., Bond, T. C., Dawidowski, L., Kholod, N., Kurokawa, J. I., Li, M., Liu, L., Lu, Z., Moura, M. C. P., O'Rourke, P. R., and Zhang, Q.: Historical (1750–2014) anthropogenic emissions of reactive gases and aerosols from the Community Emissions Data System (CEDS), Geosci. Model Dev., 11, 369-408, 10.5194/gmd-11-369-2018, 2018.

Janssens-Maenhout, G., Crippa, M., Guizzardi, D., Muntean, M., Schaaf, E., Dentener, F., Bergamaschi, P., Pagliari, V., Olivier, J. G. J., Peters, J. A. H. W., van Aardenne, J. A., Monni, S., Doering, U., Petrescu, A. M. R., Solazzo, E., and Oreggioni, G. D.: EDGAR v4.3.2 Global Atlas of the three major greenhouse gas emissions for the period 1970–2012, Earth Syst. Sci. Data, 11, 959-1002, 10.5194/essd-11-959-2019, 2019.

Kuenen, J., Dellaert, S., Visschedijk, A., Jalkanen, J. P., Super, I., and Denier van der Gon, H.: CAMS-REG-v4: a state-of-the-art high-resolution European emission inventory for air quality modelling, Earth Syst. Sci. Data, 14, 491-515, 10.5194/essd-14-491-2022, 2022.

Kuttippurath, J., Patel, V. K., Kashyap, R., Singh, A., and Clerbaux, C.: Anomalous increase in global atmospheric ammonia during COVID-19 lockdown: Need policies to curb agricultural emissions, Journal of Cleaner Production, 434, 140424, https://doi.org/10.1016/j.jclepro.2023.140424, 2024.

Li, C., Martin, R. V., Shephard, M. W., Cady-Pereira, K., Cooper, M. J., Kaiser, J., Lee, C. J., Zhang, L., and Henze, D. K.: Assessing the Iterative Finite Difference Mass Balance and 4D-Var Methods to Derive Ammonia Emissions Over North America Using Synthetic Observations, Journal of Geophysical Research: Atmospheres, 124, 4222-4236, https://doi.org/10.1029/2018JD030183, 2019.

Liu, F., van der A, R. J., Eskes, H., Ding, J., and Mijling, B.: Evaluation of modeling NO2 concentrations driven by satellite-derived and bottom-up emission inventories using in situ measurements over China, Atmos. Chem. Phys., 18, 4171-4186, 10.5194/acp-18-4171-2018, 2018.

Lolkema, D. E., Noordijk, H., Stolk, A. P., Hoogerbrugge, R., van Zanten, M. C., and van Pul, W. A. J.: The Measuring Ammonia in Nature (MAN) network in the Netherlands, Biogeosciences, 12, 5133-5142, 10.5194/bg-12-5133-2015, 2015.

Luo, Z., Zhang, Y., Chen, W., Van Damme, M., Coheur, P. F., and Clarisse, L.: Estimating global ammonia (NH3) emissions based on IASI observations from 2008 to 2018, Atmos. Chem. Phys., 22, 10375-10388, 10.5194/acp-22-10375-2022, 2022.

Menut, L., Bessagnet, B., Briant, R., Cholakian, A., Couvidat, F., Mailler, S., Pennel, R., Siour, G., Tuccella, P., Turquety, S., and Valari, M.: The CHIMERE v2020r1 online chemistry-transport model, Geosci. Model Dev., 14, 6781-6811, 10.5194/gmd-14-6781-2021, 2021.

Menut, L., Bessagnet, B., Khvorostyanov, D., Beekmann, M., Blond, N., Colette, A., Coll, I., Curci, G., Foret, G., Hodzic, A., Mailler, S., Meleux, F., Monge, J. L., Pison, I., Siour, G., Turquety, S., Valari, M., Vautard, R., and Vivanco, M. G.: CHIMERE 2013: a model for regional atmospheric composition modelling, Geosci. Model Dev., 6, 981-1028, 10.5194/gmd-6-981-2013, 2013.

Mijling, B. and van der A, R. J.: Using daily satellite observations to estimate emissions of short-lived air pollutants on a mesoscopic scale, Journal of Geophysical Research: Atmospheres, 117, 10.1029/2012JD017817, 2012.

Mijling, B., van der A, R. J., and Zhang, Q.: Regional nitrogen oxides emission trends in East Asia observed from space, Atmos. Chem. Phys., 13, 12003-12012, 10.5194/acp-13-12003-2013, 2013.

Noordijk, H., Braam, M., Rutledge-Jonker, S., Hoogerbrugge, R., Stolk, A. P., and van Pul, W. A. J.: Performance of the MAN ammonia monitoring network in the Netherlands, Atmospheric Environment, 228, 117400, https://doi.org/10.1016/j.atmosenv.2020.117400, 2020.

Pinterits, M., B. Ullrich, T. Bartmann and M. Gager: European Union emission inventory report 1990-2019 under the UNECE Convention on Long-range Transboundary Air Pollution (Air Convention), EEA Report No 5/2021, 2021NEC, Air pollution in Europe: 2023 reporting status under the National Emission reduction Commitments Directive, 2023 (https://www.eea.europa.eu/publications/national-emission-reduction-commitments-directive-2023/air-pollution-in-europe-2023), 2023.

Renard, J. J., Calidonna, S. E., and Henley, M. V.: Fate of ammonia in the atmosphere—a review for applicability to hazardous releases, Journal of Hazardous Materials, 108, 29-60, https://doi.org/10.1016/j.jhazmat.2004.01.015, 2004.

Rijsdijk, P., Eskes, H., Dingemans, A., Boersma, F., Sekiya, T., Miyazaki, K., and Houweling, S.: Quantifying uncertainties of satellite NO2 superobservations for data assimilation and model evaluation, EGUsphere, 2024, 1-42, 10.5194/egusphere-2024-632, 2024.

Schaap, M., van Loon, M., ten Brink, H. M., Dentener, F. J., and Builtjes, P. J. H.: Secondary inorganic aerosol simulations for Europe with special attention to nitrate, Atmos. Chem. Phys., 4, 857-874, 10.5194/acp-4-857-2004, 2004.

Shephard, M. W. and Cady-Pereira, K. E.: Cross-track Infrared Sounder (CrIS) satellite observations of tropospheric ammonia, Atmos. Meas. Tech., 8, 1323-1336, 10.5194/amt-8-1323-2015, 2015.

Shephard, M. W., Dammers, E., Cady-Pereira, K. E., Kharol, S. K., Thompson, J., Gainariu-Matz, Y., Zhang, J., McLinden, C. A., Kovachik, A., Moran, M., Bittman, S., Sioris, C. E., Griffin, D., Alvarado, M. J., Lonsdale, C., Savic-Jovcic, V., and Zheng, Q.: Ammonia measurements from space with the Cross-track Infrared Sounder: characteristics and applications, Atmos. Chem. Phys., 20, 2277-2302, 10.5194/acp-20-2277-2020, 2020.

Sitwell, M., Shephard, M. W., Rochon, Y., Cady-Pereira, K., and Dammers, E.: An ensemble-variational inversion system for the estimation of ammonia emissions using CrIS satellite ammonia retrievals, Atmos. Chem. Phys., 22, 6595-6624, 10.5194/acp-22-6595-2022, 2022.

Soulie, A., C. Granier, S. Darras, N. Zilbermann, T. Doumbia, M. Guevara, J.-P. Jalkanen, S. Keita, C. Liousse, M. Crippa, D. Guizzardi, R. Hoesly, and Smith, S. J.: Global Anthropogenic Emissions (CAMS-GLOB-ANT) for the Copernicus Atmosphere Monitoring Service Simulations of Air Quality Forecasts and Reanalyses, Earth Syst. Sci. Data, 2023.

Van Damme, M., Clarisse, L., Whitburn, S., Hadji-Lazaro, J., Hurtmans, D., Clerbaux, C., and Coheur, P.-F.: Industrial and agricultural ammonia point sources exposed, Nature, 564, 99-103, 10.1038/s41586-018-0747-1, 2018.

Van Damme, M., Clarisse, L., Franco, B., Sutton, M. A., Erisman, J. W., Wichink Kruit, R., van Zanten, M., Whitburn, S., Hadji-Lazaro, J., Hurtmans, D., Clerbaux, C., and Coheur, P.-F.: Global, regional and national trends of atmospheric ammonia derived from a decadal (2008–2018) satellite record, Environmental Research Letters, 16, 055017, 10.1088/1748-9326/abd5e0, 2021.

van der A, R. J., Ding, J., and Eskes, H.: Monitoring European anthropogenic NOx emissions from space, Atmos. Chem. Phys., 24, 7523-7534, 10.5194/acp-24-7523-2024, 2024.

van der A, R. J., de Laat, A. T. J., Ding, J., and Eskes, H. J.: Connecting the dots: NOx emissions along a West Siberian natural gas pipeline, npj Climate and Atmospheric Science, 3, 16, 10.1038/s41612-020-0119-z, 2020.

van der A, R. J., Mijling, B., Ding, J., Koukouli, M. E., Liu, F., Li, Q., Mao, H., and Theys, N.: Cleaning up the air: effectiveness of air quality policy for SO2 and NOx emissions in China, Atmos. Chem. Phys., 17, 1775-1789, 10.5194/acp-17-1775-2017, 2017.

van der Graaf, S., Dammers, E., Segers, A., Kranenburg, R., Schaap, M., Shephard, M. W., and Erisman, J. W.: Data assimilation of CrIS NH3 satellite observations for improving spatiotemporal NH3 distributions in LOTOS-EUROS, Atmos. Chem. Phys., 22, 951-972, 10.5194/acp-22-951-2022, 2022.

van Geffen, J. H. G. M., Eskes, H. J., Boersma, K. F., and Veefkind, J. P.: TROPOMI ATBD of the total and tropospheric NO2 data products, Report S5P-KNMI-L2-0005-RP, version 2.4.0, 202207-11, KNMI, De Bilt, The Netherlands,, https://sentinel.esa.int/documents/247904/2476257/Sentinel-5P-TROPOMI-ATBD-NO2-data-products (last access: 23 Nov. 2023), 2022.

Veefkind, J. P., Aben, I., McMullan, K., Förster, H., de Vries, J., Otter, G., Claas, J., Eskes, H. J., de Haan, J. F., Kleipool, Q., van Weele, M., Hasekamp, O., Hoogeveen, R., Landgraf, J., Snel, R., Tol, P., Ingmann, P., Voors, R., Kruizinga, B., Vink, R., Visser, H., and Levelt, P. F.: TROPOMI on the ESA Sentinel-5 Precursor: A GMES mission for global observations of the atmospheric composition for climate, air quality and ozone layer applications, Remote Sensing of Environment, 120, 70-83, http://dx.doi.org/10.1016/j.rse.2011.09.027, 2012.

White, E., Shephard, M. W., Cady-Pereira, K. E., Kharol, S. K., Ford, S., Dammers, E., Chow, E., Thiessen, N., Tobin, D., Quinn, G., O'Brien, J., and Bash, J.: Accounting for Non-Detects: Application to Satellite Ammonia Observations, Remote Sensing, 15, 2610, 2023.

Wyer, K. E., Kelleghan, D. B., Blanes-Vidal, V., Schauberger, G., and Curran, T. P.: Ammonia emissions from agriculture and their contribution to fine particulate matter: A review of implications for human health, Journal of Environmental Management, 323, 116285, https://doi.org/10.1016/j.jenvman.2022.116285, 2022.

Zavyalov, V., Esplin, M., Scott, D., Esplin, B., Bingham, G., Hoffman, E., Lietzke, C., Predina, J., Frain, R., Suwinski, L., Han, Y., Major, C., Graham, B., and Phillips, L.: Noise performance of the CrIS instrument, Journal of Geophysical Research: Atmospheres, 118, 13,108-113,120, https://doi.org/10.1002/2013JD020457, 2013.

Zhang, L., Chen, Y., Zhao, Y., Henze, D. K., Zhu, L., Song, Y., Paulot, F., Liu, X., Pan, Y., Lin, Y., and Huang, B.: Agricultural ammonia emissions in China: reconciling bottom-up and top-down estimates, Atmos. Chem. Phys., 18, 339-355, 10.5194/acp-18-339-2018, 2018.

Zhang, X., Gu, B., van Grinsven, H., Lam, S. K., Liang, X., Bai, M., and Chen, D.: Societal benefits of halving agricultural ammonia emissions in China far exceed the abatement costs, Nature Communications, 11, 4357, 10.1038/s41467-020-18196-z, 2020.

Zhu, L., Henze, D. K., Cady-Pereira, K. E., Shephard, M. W., Luo, M., Pinder, R. W., Bash, J. O., and Jeong, G.-R.: Constraining U.S. ammonia emissions using TES remote sensing observations and the GEOS-Chem adjoint model, Journal of Geophysical Research: Atmospheres, 118, 3355-3368, https://doi.org/10.1002/jgrd.50166, 2013.